Semicond. Sci. Technol. **11** (1996) 380–387. Printed in the UK

Monte Carlo analysis of a Schottky diode with an automatic space-variable charge algorithm

M J Martín, T González, D Pardo and J E Velázquez

Departamento de Física Aplicada, Facultad de Ciencias, Universidad de Salamanca, 37008 Salamanca, Spain

Received 22 March 1995, in final form 14 November 1995, accepted for publication 14 November 1995

Abstract. An efficient one-dimensional ensemble Monte Carlo simulator that improves the study of carrier transport by including a space-variable charge algorithm has been developed. The algorithm is automatically implemented in regions with remarkable concentration gradients. In this way is possible to study devices in which the carrier concentration varies by several orders of magnitude along the device and/or when we are interested in the population of states rarely occupied by the carriers (tails of distribution functions, hot electrons, etc) without excessive CPU requirements.

In the present work this technique is used to study a Schottky barrier diode over a wide range of forward bias (80–800 mV). In particular, the exponential behaviour of the current–voltage characteristic, the agreement of this with the experimental results, the distribution function and the recombination velocity of carriers close to the metal–semiconductor interface confirm the validity of the implemented algorithm.

1. Introduction

The ensemble Monte Carlo method (EMC) is a powerful tool for simulating submicrometre semiconductor devices because it affords a very complete data set on their carrier transport properties [1, 2]. However, the major drawbacks to the EMC approach derive from the fact that much CPU time is required when the carrier concentration varies by several orders of magnitude along the device and when unlikely high-energy carrier states are to be studied [3, 4]. Thus, study of the degrading effect in the MOSFET channel due to the energetic electrons ('hot electrons') is of crucial importance in the performance of the device [5, 6]. In this sense it is very important that the EMC should be able to predict small substrate and gate currents. In bipolar transistors, study of the heating of electrons when these cross the base–collector depletion region of high electric fields is essential. Calculation of 'rare' electron states is of great relevance in 'barrier-controlled current' devices because in these the probability of a carrier crossing the space-charge region (SCR) falls exponentially with the opposing barrier height.

The aim of the present work is to report the results obtained in a one-dimensional EMC simulation of a barrier-controlled device. To ensure statistical validity of the results obtained in the SCR, a procedure of space-variable charge was implemented. The main features of the method used are reported in section 2.

A Shottky barrier diode (SBD) was chosen as the 'barrier-controlled current device' owing to its special characteristics, namely (i) an SCR with a low free carrier concentration and (ii) a small number of carriers with enough energy to surmount the barrier. Additionally, charge transport in SBDs is applicable to similar problems such as conduction band spikes in heterojunction bipolar transistors (HBTs) [7].

Section 3 reports on the simulated structures, boundary conditions and parameters employed in the simulation. Section 4 offers a comparison between the results of a standard EMC simulation (EMC I) and those obtained in an EMC simulation in which the space-variable charge procedure is implemented (EMC II). The EMC II results are compared with the current theories and existing experimental results. Finally, section 5 presents the main conclusions.

2. Description of the space-variable charge procedure

By means of a traditional EMC scheme [3], most of the sample particles will populate the highly doped regions of the device (generally close to ohmic contacts with a small influence on the device behaviour), requiring considerable CPU time for the simulation. The small population of sample particles in the low-density regions or SCR leads

0268-1242/96/030380+08$19.50

to strong fluctuations in the average results (velocity, energy...).

In order to overcome these difficulties, different statistical improvements of the standard Monte Carlo technique have been introduced. In 1977 Phillips and Price [8] developed a weighting procedure of statistical enhancement based on dividing the 'history' of the electron in a semiconductor into two parts: containing the 'common' and the 'rare' states (energy states greater than a threshold value). By implementing a repetition scheme varying in duration, these authors calculated the energy distribution function for hot electrons in a semiconductor.

In 1985, Wang *et al* [9] developed an EMC based on the work in [8], assigning an energy-dependent weight to each 'sample-electron'. That EMC code was applied to a planar-doped barrier (PBD) structure of GaAs of 0.2 μm length with a barrier height of 0.25 V. The PBD structure presents an extreme concentration ratio of 10^5.

The Phillips and Price technique was used by Sangiorgi *et al* [5] to study transport in a MOSFET channel. The domain of the 'rare' states of the electron is divided into a number of 'subregions' where a multiple repetition scheme with different multiplication factors is implemented in a drift-diffusion method coupled with a single-particle Monte Carlo algorithm.

Fischetti and Laux also made use of that scheme to improve their two-dimensional EMC in a study of S_i n and p MOSFETs, GaAs MESFETs and S_i bipolar transistors by the definition of 'stat-box' regions in real and k-space [5, 10]. In this procedure, the statistical variance of each 'rare' state is controlled by automatically adjusting the number of particles in 'rare configurations'.

A weighting technique similar to that of Wang *et al* [9] has also been used by Maziar and Lundstrom [11] to study the recombination velocity at the metal–semiconductor interface of a GaAs SBD. The semiconductor employed is homogeneous (10^{17} cm^{-3}) and the 'sample electrons' were injected into the SCR of the diode by a weighted Maxwellian distribution function. Although they used the weighting scheme, the study is limited to conditions of a semiconductor–metal barrier height of a few $K_{\mathrm{B}}T/q$.

On studying semiconductor devices it is usual to employ an EMC method with a constant particle factor (EMC I) [12]: each sample carrier has a preset and constant electron-particle equivalent (EPE). That EPE (in one-dimensional Monte Carlo) records the number of electrons per unit area, in the two unsimulated dimensions, that represents a simulated sample particle. A variable EPE that depends of the position occupied by the simulated particle along the device allows that the lightly populated regions have similar statistical significance than the more populated ones.

Initially, the device is divided into several regions of different charge-particle weight: $S_i, i = 1, 2, \ldots, n$ such that each of these n regions is assigned a different value of electron-particle equivalent, EPE_i.

The space-variable charge procedure aims at achieving physically appropiate expansion/compression processes between adjacent regions (S_i, S_{i+1}). When a particle undergoes a transition from one state $(r, \boldsymbol{k})$ of a region S_i to another state $(r', \boldsymbol{k}')$ in a region S_{i+1} of less probable population (hence $\mathrm{EPE}_{i+1} < \mathrm{EPE}_i$), a multiplication algorithm of this particle is activated. The expansion factor N_i is given with the ratio between the EPE of the final and initial regions. The algorithm must generate N_i particles, ensuring that together with the 'parent' particle, that is removed, the laws of energy and momentum conservation are fulfilled (figure 1 upper part). To solve Poisson's equation and calculate the average values of the simulation, the generated particles acquire the charge weight conferred by the EPE of the new region. An inverse process of compression must be carried out in the case in which the final state corresponds to a more probable population region (figure 1, lower part).

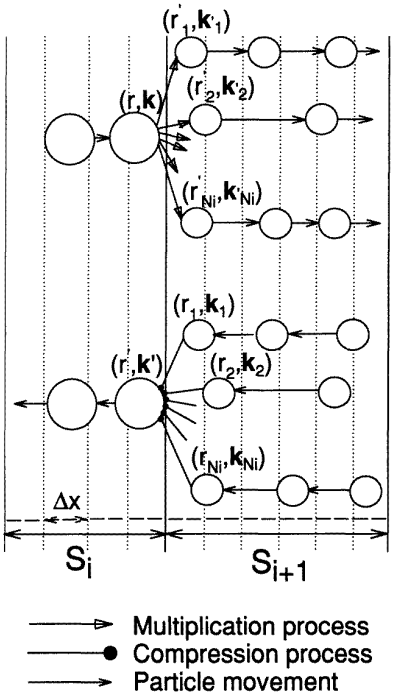

Figure 1. Schematic drawing of expansion/compression processes between states of adjacent regions S_i and S_{i+1} for the case in which $\mathrm{EPE}_{i+1} < \mathrm{EPE}_i$. Each node represents an electron state. Full lines indicate the regions of different EPE and dotted lines the mesh for the resolution of the Poisson equation (Δx is the cell width). The multiplication factor associated with this particular transition is N_i.

To facilitate the implementation of this space-variable charge algorithm, the limits of the expansion/compression regions must coincide with the boundaries of the cells used to solve Poisson's equation. Neither the position of the boundaries of the variable charge regions nor the best values of each EPE are known at the start of the simulation since they depend on the applied voltage.

With the aim of achieving a number of sample particles practically equal in each cell, at the beginning of the simulation the program performs an iterative autoadjust algorithm. This algorithm is coupled to the EMC scheme and provides an automatic assignment of the EPE values and boundaries of the different expansion/compression regions. For each bias point, this algorithm carries out

modifications in the EPE of each cell until a stationary situation is reached. It is based on the relation between the potential gradient and the free carrier concentration along the device. In broad outline the algorithm is as follows.

We initiate the ensemble simulation by assigning to each cell j a rough EPE_j value which is determined by

$$\mathrm{EPE}_j = \frac{\Delta x_j \mathrm{DOP}_j}{\mathrm{NP}_j} \tag{1}$$

where Δx_j is the cell width, DOP_j the doping density and NP_j the number of particles of the j-cell. The values of NP_j at each cell are set as similar as possible. By comparison of the EPE values of adjacent cells we determine the boundaries of the S_i regions and the N_i factors. The EPE values are adjusted in order to keep the integer nature of N_i.

As second step we perform an usual EMC calculation (with these EPE_j values) during an adequate number of iterations (1–5 ps) until an accurate enough calculation of the potential profile is reached. This potential profile is necessary to obtain a free carrier density estimation which will be used to achieve a more adequate EPE at each cell. Let us consider two cells: j, k. Near equilibrium conditions (low current level) and/or when the j and k cells are spatially close we can assume that the quasi-Fermi potentials of the electrons in both cells are equal. In consequence we can express

$$n_k \approx n_j \exp\left(\frac{V_k - V_j}{K_\mathrm{B}T/q}\right) \tag{2}$$

where n is the free carrier density and V the value of the potential previously calculated.

This approximation is suitable to obtain, taking the origin of n and V in the highly doped region, an estimated value of the free carrier density along the device. This allows us to recalculate the new EPE of each cell using n_k instead of DOP_k in (1) and then determine the new position of the boundaries of the S_i regions and the new N_i factors. Again the integer nature of N_i must be kept. This requirement leads to an EPE profile formed of discrete values which are multiples of each other. These EPE values may not be consistent with the initial NP_j, i.e. the time average of simulated particles at each cell $\overline{\mathrm{NP}_j}$ could be different from the initial NP_j.

In order to correct these discrepancies between $\overline{\mathrm{NP}_j}$ and NP_j, further modifications of S_i and N_i are made (from the results of simulations of 500–1000 iterations) until $\overline{\mathrm{NP}_j}$ and NP_j coincide within a 40% tolerance. This iterative procedure performs an adaptive optimization of the S_i boundary positions and the N_i factors.

This procedure enables the EMC method to be used for the study of charge transport in devices with regions of very different doping levels (BJTs, HBTs, ...), thus considerably reducing the number of sample particles in regions of high doping density and at the same time obtaining reliable statistics of 'rare processes' such as the high-energy tails of the distribution functions.

3. Schottky barrier diode. One-dimensional ensemble Monte Carlo simulator

Currently, SBDs continue to be widely used, due to their excellent behaviour at high frequencies (mixers and detectors extend to up to frequencies of several hundred gigahertz [13, 14]).

Over the past 40 years, the current–voltage characteristics of this type of diode have been extensively dealt with in the literature: Crowell, Chang and Sze developed a theory to calculate the current flow of majority carriers in metal–semiconductor barriers by encompassing the Schottky diffusion and Bethe thermoionic emission theories within a single thermoionic emission diffusion (TED) theory that includes the image force lowering of the barrier [15] and tunnelling [16] effects. More recently, several numerical analysis [17–21] and Monte Carlo simulations [11, 22–24] have been performed with a view to studying charge transport and current fluctuations in SBDs.

The study of a forward biased SBD with the semiconductor–metal barrier greater than 2–3 $K_\mathrm{B}T/q$ is a problem for an EMC algorithm with constant EPE [11, 24]. In that operation the number of carriers surmounting the barrier is too small to ensure the reliability of the current calculation without an extensive amount of CPU time.

The simulated SBD is modelled as Si n^+-n-metal structure. The absence of two-dimensional effects is assumed. The doping of the n^+ region is 10^{17} cm^{-3} and it is 0.3 μm long. The simulated electrode in the free end of the n^+ region is modelled as an ideal ohmic contact: the free carrier concentration of a small region close to the contact should remain constant and equal to the doping density [25]. Periodically, sample particles are injected into the electrode at thermal equilibrium with a velocity chosen randomly according to a Maxwellian distribution function weighted by the velocity component perpendicular to the contact and directed into the device. The simulation has been carried out with two different doping densities (N_D) of the n region (10^{15} cm^{-3} and 10^{16} cm^{-3}), that is 0.8 μm long. The Schottky barrier is situated at the end of this n zone with the metal contact acting as a perfect absorbing boundary. Electrons with sufficient velocity (kinetic energy) to pass the energy barrier are injected into the metal. No carrier is injected from the metal into the semiconductor which imposes a lower limit ($3K_\mathrm{B}T/q \approx 80$ mV) on the range of applied voltages in the simulation.

The quantum effects of tunnelling and barrier reflection in the semiconductor–metal contact are not included in the simulation. Image-force lowering effect is not taken into account globally, only its effects at low bias, as will be detailed below. Figure 2 shows the energy band diagram of the SBD under equilibrium conditions.

The barrier height, Φ_Bn of the metal (Au)–S_i(n-type) contact is an important factor to be taken into account in the EMC simulation. We assume that Φ_Bn remains constant with bias. The value of Φ_Bn has been calculated from experimental results [16], using the extraction method of the Schottky diode parameters from the forward current–voltage characteristics [26]. The barrier height considered is 0.81 eV, which lies within the range reported in

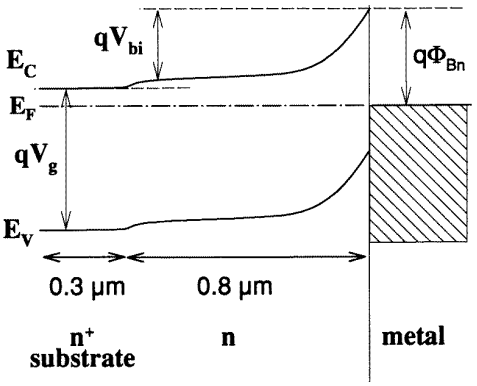

Figure 2. Detailed band diagram of a metal–semiconductor Schottky barrier diode under equilibrium conditions.

experimental results [16, 27]. Therefore the barrier height from the n region to the metal (built-in potential: qV_{bi}) is equal to 0.54 eV and 0.60 eV for doping densities of 10^{15} cm^{-3} and 10^{16} cm^{-3} respectively.

The S_i microscopic model employed is the same as that reported in [28]. The simulation was performed at 296 K. The calculation of the physical quantities of interest follows the standard scheme [1]. Self-consistent coupling of the Poisson solver algorithm with an EMC simulator (one-dimensional in real space and three-dimensional in k-space) affords the spatial distribution of the electric potential. The device is divided into equal cells of 100 Å each, that are sufficiently small to reproduce the spatial variations in the electric potential. The time step, DT, to solve the Poisson equation is 10 fs. The EPE value used in the EMC I simulation is 10^{13} electrons/m^2.

4. Results

The current–voltage characteristics under forward bias conditions obtained with the EMC I and EMC II simulations are shown in figures 3(a) and 3(b) respectively. The results of both simulations have been obtained with the same simulation time.

For high forward voltages, no significant differences in the values of current density between EMC I (figure 3(a)) and EMC II (figure 3(b)) are seen for either of the dopings of the n region since the SCR are negligible due to the effects of the disappearance of the barrier. This confirms the consistency of the space-variable charge scheme.

Only the forward bias range leading to a semiconductor–metal barrier height lower than a few K_BT/q can be reliably simulated in acceptable CPU times by the EMC I method. The poor number of sample particles crossing the SCR is responsible for the lack of precision appearing in the current values as the voltage decreases (see error bars). For the sake of clarity, the error bars are only represented for the n region doping of 10^{16} cm^{-3}. It should be noted that using the EMC I method for the lower bias (0.37 V) over 300 ps of simulation, no sample particle was seen to cross the semiconductor–metal contact, whereas using the EMC II method for the same simulation

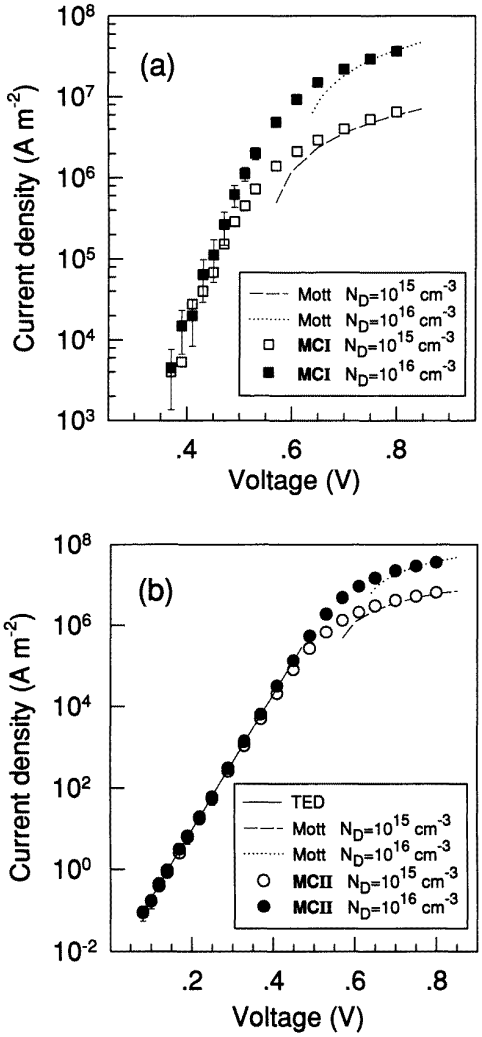

Figure 3. Current–density characteristics obtained with the EMC I (a) and the EMC II (b) simulations for two doping densities of the n region: 10^{15} cm^{-3} (open symbols) and 10^{16} cm^{-3} (full symbols). The Mott (broken and dotted curves) and the TED (solid curve) predictions are also plotted in the figures.

conditions we found that around 7500 particles crossed the semiconductor–metal contact.

Figures 4(a) and (b) show respectively the spatial distributions of carrier density and mean energy obtained with EMC I and EMC II simulations using the same number of time steps. Owing to the insufficient number of particles in the SCR when the EMC I simulation is used, strong spatial fluctuations appear in the average values. Accordingly, henceforth the results described correspond to simulations performed with the EMC II method.

For applied voltages (V_{apl}) to above V_{bi} the current tends to show a quasilinear dependence on voltage due to the disappearance of the barrier (figure 3). Essentially, the diode behaves as the series resistance associated with the n and n^+ regions, that controls the current through the device [29]. Figure 3(b) plots the current–voltage characteristics according to the Mott theory [30] for both doping densities. The EMC II results tend to the Mott predictions and are in

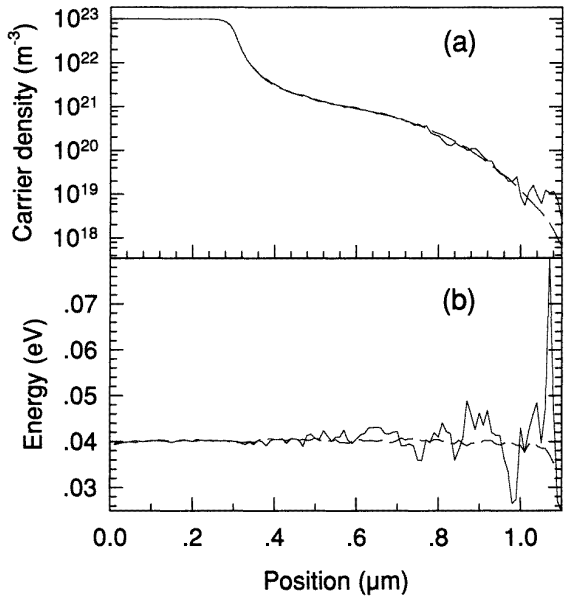

Figure 4. Comparison between the profiles of carrier density (*a*) and mean energy (*b*) obtained with the EMC I (full curve) and the EMC II (broken curve) simulations as a function of the position in the SBD for a bias of 0.37 V.

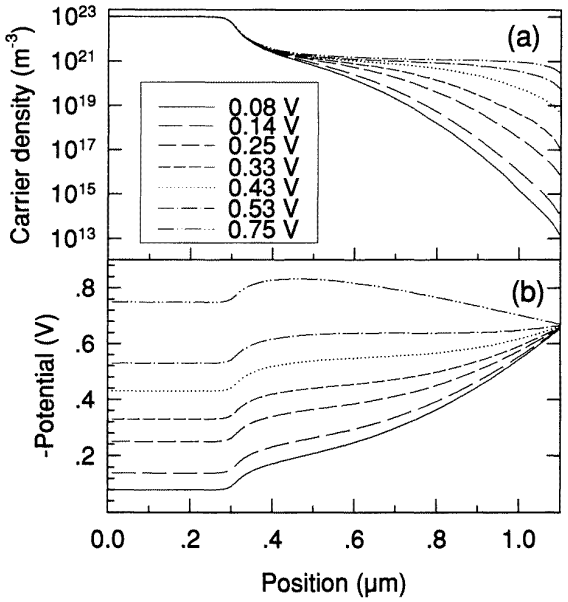

Figure 5. Profiles of free-carrier density (*a*) and potential (*b*) as a function of the position along the SBD with the n zone doping density equal to 10^{15} cm^{-3} for different biases. The key given in (*a*) is also valid for (*b*).

excellent agreement with them for $V_{apl} > 0.65$ V.

For forward biases lower than flat band conditions ($V_{apl} \approx V_{bi}$), the current exhibits an exponential type of behaviour determined by the thermoionic emission and diffusion processes. The exponential current–voltage dependence corresponding to a 'barrier-controlled current' appears over a wide range of 80 mV $< V_{apl} <$ 470 mV (figure 3(*b*)).

The expansion/compression scheme is applied automatically in the regions in which there are remarkable concentration gradients such as n^+–n interfaces and mainly the SCR of the metal–semiconductor union. To determine the static characteristics in the exponential range, a varying number of expansion/compression regions was used, depending on the n-region doping density and the forward bias.

At low bias the validity of the results thus obtained is limited to the appearance of phenomena such as generation–recombination processes [31] and minority carrier injection [32], not taken into account in the simulation.

In the exponential region of the current–voltage curves we do not observe significant differences between the current–voltage characteristics for both doping densities of the n region. In theory, the value of the saturation current does not depend on impurity concentration. Fitting of the EMC II results to the TED theory affords a saturation current of 4.25×10^{-3} A m^{-2} and a non-ideality factor of 1.01, both within the range of experimental values [16]. This fitting of the TED theory is also plotted in figure 3. Additionally, this value for saturation current value agrees with the theoretical predictions for Si at this temperature.

The carrier density and potential profiles are shown in figures 5(*a*) and 5(*b*) for an n-region doping density of 10^{15} cm^{-3}, and in figures 6(*a*) and 6(*b*) for 10^{16} cm^{-3}.

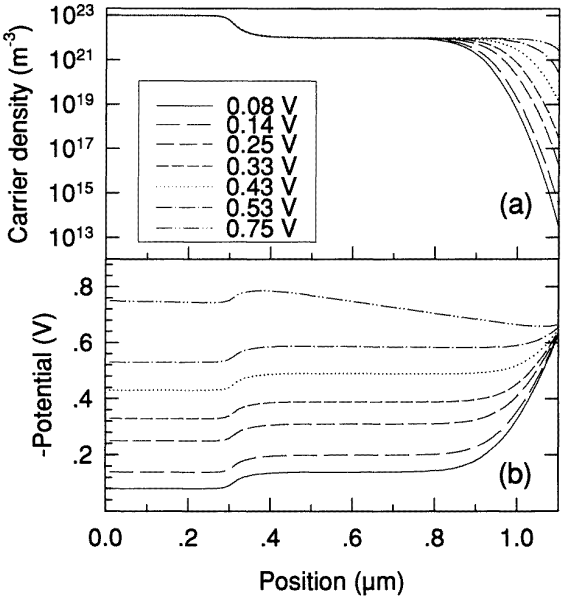

Figure 6. Profiles of free-carrier density (*a*) and potential (*b*) as a function of the position along the SBD with the n zone doping density equal to 10^{16} cm^{-3} for different biases.

In the plots of the potential, it may be seen that when $V_{apl} > V_{bi}$ the barrier disappears and the voltage drops along the whole device and mainly along the n region (more resistive), in agreement with the observed resistive behaviour. When $V_{apl} < V_{bi}$ the whole of the potential drop is essentially localized in the region close to the metal–semiconductor interface.

The carrier density profiles corroborate the existence of a depletion region near to the Schottky contact. Use

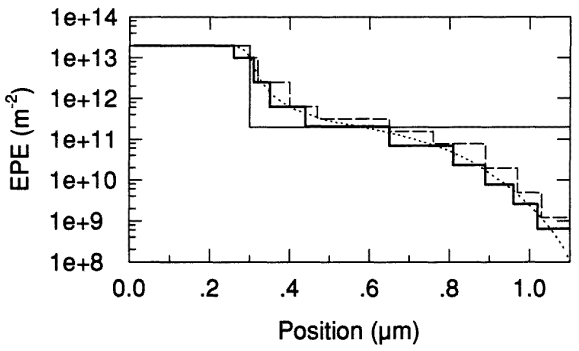

Figure 7. Different EPE profiles generated by the iterative autoadjust algorithm in the simulation of the structure with a doping density in the n region of 10^{15} cm^{-3} for a bias of 0.37 V. Full line: rough initial EPE assignment provided by equation (1) with NP_j of 50. Dotted line: EPE assignment provided by equation (1) with n_j instead DOP_j. Broken line: first approach of a discrete profile to fit the previous curve. Bold line: final EPE assigment.

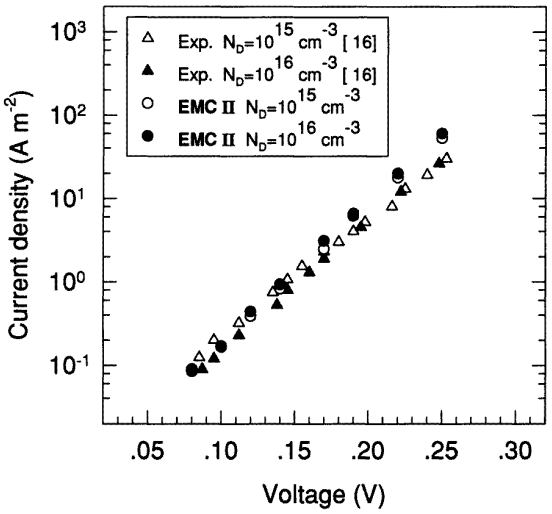

Figure 8. Comparison between current–density characteristics obtained with the EMC II simulation (circles) and the experimental results taken from [15] (triangles), for both n-zone doping densities: 10^{15} cm^{-3} (open symbols) and 10^{16} cm^{-3} (full symbols).

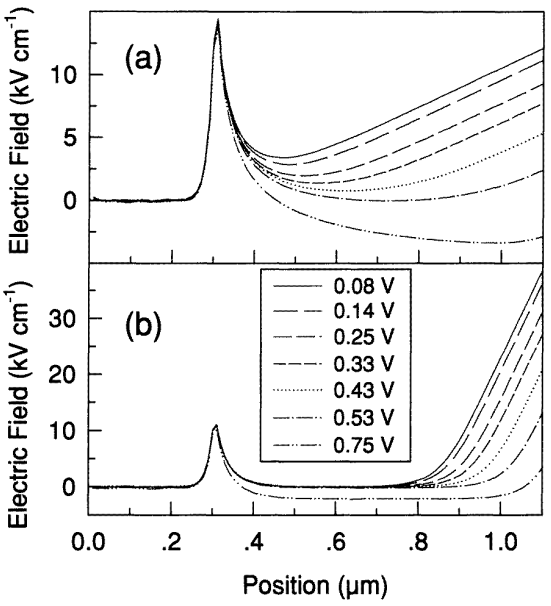

Figure 9. Electric field profile as a function of the position along the SBD with the n-zone doping density equal to 10^{15} cm^{-3} (*a*) and 10^{16} cm^{-3} (*b*) for different biases.

of the space-variable charge algorithm has been completely satisfactory for both doping densities due to the absence of spatial fluctuations in the concentration profile even though the carrier concentration varies more than 10 orders of magnitude across the device.

It may be seen that the SCR width is almost all of the n region for a doping density of 10^{15} cm^{-3}, also, the carrier concentration decreases gradually with the distance as the Schottky contact is approached. In the 10^{16} cm^{-3} structure, the SCR width is approximately 0.3 μm and the decrease in the carrier concentration is much sharper. As a consequence of that, the width of the expansion/compression regions in the SCR must decrease as the doping density increases. To obtain an almost constant number of sample particles in each cell (approximately 50) it has been necessary to consider a different number of regions depending on the bias: from seven regions for V_{apl} of 0.47 V to 17 regions for 80 mV. Figure 7 shows an example of the iterative autoadjust algorithm explained in section 2 applied to the structure with a doping density in the n region of 10^{15} cm^{-3} for V_{apl} of 0.37 V. The iterative application of the automatic algorithm finally provides the boundaries and the EPE values of 10 different expansion/compression regions that are shown in the figure.

Figure 8 shows the EMC II results for the lowest electric fields applied as compared with the values taken from [16] in the ⟨111⟩ direction for both doping densities. The excellent agreement between the EMC II simulations and the experimental results for the lowest bias (80–170 mV) can be seen. For higher voltages (170–250 mV) the EMC II results are somewhat larger than the experimental ones. There are two reasons for this slight difference:

(i) The barrier height Φ_{Bn} was held constant during the simulation. The dependence of the 'barrier lowering' on the electric field at the metal–semiconductor contact has not been taken into account. As the voltage increases, the electric field at the interface decreases (figure 9) and makes the barrier height increase slightly.

(ii) Additional discrepancies appear due to the different values of the series resistances of the simulated structure and the experimental one.

Owing to the high number of particles close to the barrier, the EMC II method is able to provide reliable energy and velocity carrier distribution functions at the metal–semiconductor interface that are not possible to achieve with EMC I.

The theoretical model most frequently used for the study of Schottky diodes is based on the TED theory [15]. Current flow near the Schottky contact can be described

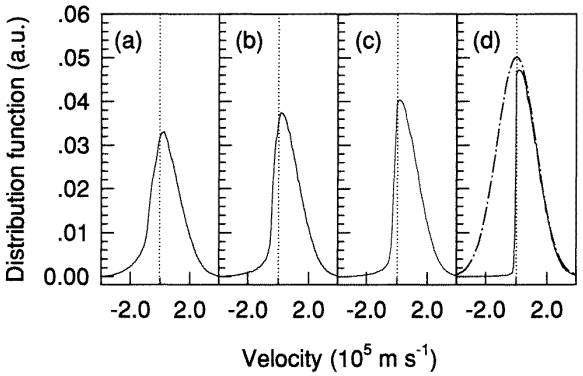

Figure 10. Velocity distribution functions of the carriers in different regions of the SCR for a bias of 0.51 V. With the space origin taken at the metal–semiconductor contact, the different regions are located: from 150 to 200 Å (*a*), from 40 to 60 Å (*b*), from 5 to 40 Å (*c*) and from 0 to 5 Å (*d*). A full-Maxwellian distribution is also plotted in (*d*) (see text).

in terms of an effective recombination velocity V_r. If the electron distribution is considered to be Maxwellian [15], this recombination velocity is given by

$$v_r = \sqrt{\frac{K_B T}{2\pi m^*}}. \tag{3}$$

Later, Baccaranni and Mazzone [22] proposed a hemi-Maxwellian velocity distribution function of electrons, for which the recombination velocity can be expressed as

$$v_r = \sqrt{\frac{2K_B T}{\pi m^*}}. \tag{4}$$

The work by Adams and Tang [18] also suggests that the interface recombination velocity should be considered as bias dependent.

During the EMC II simulation, the carrier distribution functions at different regions of the SCR are calculated. Also the mass and velocity of the carriers at a distance of less than 5 Å from the metal–semiconductor barrier were calculated to verify the estimation of the recombination velocity. Owing to the perfectly absorbing nature of the Schottky contact, and because metal–semiconductor injection is not considered, the distribution function close to the contact does not contain carriers with negative velocities. Thus, on approaching the metal–semiconductor interface, the velocity distribution function of electrons changes from a full Maxwellian to a hemi-Maxwellian. This effect can be appreciated for a bias of 0.51 V in figures 10(*a*)–(*d*). The distribution function of the carriers in each of the X valleys of our Si band model are identical (as would correspond to the isotropic behaviour of Si with the field applied in the ⟨111⟩ direction). No bias dependence of the recombination velocity was found. The velocity value obtained (9.8×10^4 m s^{-1}) is consistent with that estimated by equation (4). Figure 10(*d*) also shows the full-Maxwellian distribution function (with m^* calculated from the simulation) for comparison with the distribution function obtained in the EMC II simulation close the Schottky contact.

5. Conclusions

In this paper an efficient one-dimensional ensemble Monte Carlo (EMC) simulator that improves the study of the carrier transport by including a spatially variable charge algorithm has been developed (EMC II). The model allows the simulation of devices in which the carrier concentration varies by several orders of magnitude along the device and/or when one is interested in the population of states rarely occupied by carriers (tails of distribution functions, hot electrons, etc).

In particular, in this work the scheme (EMC II) was used to study a Schottky barrier device for a broad range of forward bias (80–800 mV). In the regions with a elevated carrier density gradients the program performs a self-fitting algorithm to optimize this scheme automatically.

The current values obtained with the EMC II simulation are consistent with the experimental data. For applied voltages above flat band conditions, the EMC II simulation results approach the Mott predictions. The exponential behaviour of the current–voltage characteristics over a wide range of bias (80–470 mV) is observed. The saturation current is in excellent agreement with the thermoionic-emission diffusion theory and the experimental results.

Because of the absence of fluctuations in the analysis of the concentration profiles, the stability of the variable charge assignation scheme is guaranteed even through the carrier concentrations vary more than 10 orders of magnitude across the device.

The number of particles close to the barrier is sufficiently high to afford a reliable carrier energy or velocity distribution functions at the metal–semiconductor interface. As the interface is approached, the variation of the velocity distribution function from a full Maxwellian to a hemi-Maxwellian is confirmed. The recombination velocity lies within the range reported in theoretical results and does not show bias dependence.

Acknowledgment

This work has been supported by the project TIC95-0652 from the CICYT.

References

[1] Jacoboni C and Lugli P 1989 *The Monte Carlo Method for Semiconductor Device Simulation* (Vienna: Springer)
[2] Constant E 1986 *Physics of Submicron Semiconductor Devices* ed H L Grubin *et al* (New York: Plenum)
[3] Hockney R and Eastwood J 1981 *Computer Simulation Using Particles* (New York: McGraw-Hill)
[4] Lugli P 1993 *Compound Semiconductor Device Modelling* ed C M Snowden and R E Miles (London: Springer) p 218
[5] Sangiorgi E, Ricco B and Venturi F 1988 *IEEE Trans. Computer-Aided Design* **7** 259
[6] Laux S E, Fischetti M V and Frank D J 1990 *IBM J. Res. Develop.* **34** 466
[7] P M Asbeck 1990 *High-speed Semiconductor Devices* ed S M Sze (New York: Wiley-Interscience) p 335
[8] Phillips A and Price P J 1977 *Appl. Phys. Lett.* **30** 528

[9] Wang T, Hess K and Iafrate G J 1985 *J. Appl. Phys.* **58** 857
[10] Fischetti M and Laux S 1988 *Phys. Rev.* B **38** 9721
[11] Maziar C M and Lundstrom M S 1987 *Electron. Lett.* **23** 61
[12] Moglestue C 1993 *Monte Carlo Simulation of Semiconductor Devices* (London: Chapman and Hall)
[13] Crowe T W, Mattauch R J, Röser H P, Bishop W L, Peatman W and Liu X 1992 *Proc. IEEE* **80** 1827
[14] Erickson N R 1992 *Proc. IEEE* **80** 1721
[15] Crowell C R and Sze S M 1966 *Solid-State Electron.* **9** 1035
[16] Chang C Y and Sze S M 1970 *Solid-State Electron.* **13** 727
[17] Guo S F 1984 *Solid-State Electron.* **6** 537
[18] Adams J and Tang T-W 1986 *IEEE Electron Device Lett.* **9** 525
[19] Hwang C G and Dutton R W 1988 *IEEE Trans. Computer-Aided Design* **7** 578
[20] Racko J, Donoval D, Barus M, Nagl V and Germanova A 1991 *Solid-State Electron.* **35** 913
[21] Bhapkar U V and Mattauch R J 1993 *IEEE Trans. Electron. Devices* **40** 1038
[22] Baccaranni G and Mazzone A M 1976 *Electron. Lett.* **12** 59
[23] Ravaioli U, Lugli P, Osman M A and Ferry D K 1985 *IEEE Trans. Electron. Devices* **32** 2097
[24] González T, Pardo D, Varani L and Reggiani L 1993 *Appl. Phys. Lett.* **63** 3040
[25] Laux S E and Fischetti M V 1991 *Monte Carlo Device Simulation: Full Band and Beyond* ed K Hess (Boston: Kluwer) p 16
[26] Cheung S K and Cheung N W 1986 *Appl. Phys. Lett.* **49** 2
[27] Van Otterloo J D 1981 *Surf. Sci. Lett.* **104** L205
[28] Martin M J, González T Pardo D and Velázquez J E 1994 *Semicond. Sci. Technol.* **9** 1316
[29] Barus M and Donoval D 1993 *Solid-State Electron.* **36** 969
[30] Mott N F 1938 *Proc. Camb. Phil. Soc.* **34** 568
[31] Yu A Y C and Snow E H 1968 *J. Appl. Phys.* **39** 3008
[32] Scharfetter D L 1965 *Solid-State Electron.* **8** 299